© 2019. Published by The Company of Biologists Ltd | Development (2019) 146, dev178632. doi:10.1242/dev.178632

H3K27me3-mediated silencing of structural genes is required for zebrafish heart regeneration

Raz Ben-Yair[1,2], Vincent L. Butty[3], Michele Busby[4], Yutong Qiu[5], Stuart S. Levine[3], Alon Goren[4,5,*], Laurie A. Boyer[3,*], C. Geoffrey Burns[1,2,6,*] and Caroline E. Burns[1,2,6,7,*]

ABSTRACT

Deciphering the genetic and epigenetic regulation of cardiomyocyte proliferation in organisms that are capable of robust cardiac renewal, such as zebrafish, represents an attractive inroad towards regenerating the human heart. Using integrated high-throughput transcriptional and chromatin analyses, we have identified a strong association between H3K27me3 deposition and reduced sarcomere and cytoskeletal gene expression in proliferative cardiomyocytes following cardiac injury in zebrafish. To move beyond an association, we generated an inducible transgenic strain expressing a mutant version of histone 3, H3.3^{K27M}, that inhibits H3K27me3 catalysis in cardiomyocytes during the regenerative window. Hearts comprising H3.3^{K27M}-expressing cardiomyocytes fail to regenerate, with wound edge cells showing heightened expression of structural genes and prominent sarcomeres. Although cell cycle re-entry was unperturbed, cytokinesis and wound invasion were significantly compromised. Collectively, our study identifies H3K27me3-mediated silencing of structural genes as requisite for zebrafish heart regeneration and suggests that repression of similar structural components in the border zone of an infarcted human heart might improve its regenerative capacity.

KEY WORDS: Zebrafish, Heart regeneration, Cardiomyocyte, Proliferation, Epigenetic, Chromatin, H3K27me3, Cardiovascular

INTRODUCTION

Shortly after birth, mammalian cardiomyocytes exit the cell cycle and lose the ability to proliferate in response to injury (Laflamme and Murry, 2011; Vivien et al., 2016). By contrast, adult zebrafish and neonatal mouse hearts complete near-perfect regeneration following tissue loss, as their cardiomyocytes retain the capacity to divide (Jopling et al., 2010; Kikuchi et al., 2010; Porrello et al., 2011; Poss et al., 2002; Raya et al., 2003). In both cases, cardiomyocytes near the injury site undergo dramatic changes in gene expression concomitant with loss of cell adhesion (Jopling et al., 2010; O'Meara et al., 2015), sarcomere disassembly (Ahuja et al., 2004; Jopling et al., 2010; Kikuchi et al., 2010; Zhang et al., 2013) and detachment from the remodeling extracellular matrix (ECM) (Bassat et al., 2017), which leaves them poised to divide and give rise to new muscle cells that colonize the wound. However, the transcriptional changes and chromatin dynamics that drive regenerative cardiomyocyte proliferation remain unclear.

Tri-methylation (me3) of lysine (K) 4 and 27 on histone (H) 3 have been relatively well characterized for their opposing roles in transcriptional output. Specifically, H3K4me3 is catalyzed by trithorax group proteins and are associated with open chromatin and active transcription (Harikumar and Meshorer, 2015). By contrast, H3K27me3 modifications, which are enzymatically deposited by polycomb repressive complex 2 (PRC2), are enriched over transcriptionally repressed loci (Harikumar and Meshorer, 2015). Interestingly, each mark shows dynamic patterns during *in vitro* cardiomyocyte differentiation from mouse and human embryonic stem cells (Paige et al., 2012; Wamstad et al., 2012). Consistent with a role for H3K27me3 dynamics, the PRC2 catalytic enzymes Ezh1 and Ezh2 perform partially redundant functions in regulating cardiomyocyte proliferation during murine cardiac development (Ai et al., 2017). Although Ezh2 is not essential for heart regeneration in mice (Ahmed et al., 2018; Ai et al., 2017), Ezh1/2 double knockouts die perinatally, leaving open a possible role for PRC2-dependent gene silencing during organ renewal. Based on these collective observations, we hypothesized that similar epigenetic mechanisms involving H3K4me3 and H3K27me3 dynamics might regulate injury-induced cardiomyocyte proliferation and regeneration in adults.

Using a combination of high-throughput transcriptional and chromatin analyses with functional follow-up studies in zebrafish, we discovered an essential role for cardiomyocyte-specific H3K27me3-mediated repression of genes encoding key structural components for successful organ renewal. Specifically, our profiling studies identified a strong correlation between reduced expression of genes encoding sarcomeric and cytoskeletal proteins and increased H3K27me3 over their loci following injury. Importantly, blocking H3K27me3 catalysis in zebrafish cardiomyocytes after injury results in regenerative failures *in vivo*. Collectively, our study identifies abnormal sarcomere persistance as a significant barrier to heart regeneration in zebrafish and suggests that dampening expression of similar structural components in the human heart might improve its regenerative capacity.

RESULTS AND DISCUSSION

To identify the transcriptional changes associated with cardiomyocyte proliferation, we performed RNA-sequencing (RNA-seq) of EGFP^{+} cardiomyocytes isolated from *gata4:EGFP* transgenic animals that were previously shown to activate *gata4* regulatory sequences following injury in highly proliferative cardiomyocytes that give rise to the regenerated tissue (Kikuchi et al., 2010). Although previously

[1]Cardiovascular Research Center, Massachusetts General Hospital, Charlestown, MA 02129, USA. [2]Harvard Medical School, Boston, MA 02115, USA. [3]Departments of Biology and Biological Engineering, Massachusetts Institute of Technology, 77 Massachusetts Avenue, Cambridge, MA 02139, USA. [4]The Broad Institute of MIT and Harvard, Cambridge, MA 02142, USA. [5]Department of Medicine, University of California San Diego, La Jolla, CA 92093, USA. [6]Department of Cardiology, Boston Children's Hospital, Boston, MA 02115, USA. [7]Harvard Stem Cell Institute, Cambridge, MA 02138, USA.

*Authors for correspondence (agoren@ucsd.edu; lboyer@mit.edu; geoff.burns@childrens.harvard.edu; caroline.burns@childrens.harvard.edu)

M.B., 0000-0003-1731-288X; A.G., 0000-0001-5669-9357; L.A.B., 0000-0003-3491-4962; C.G.B., 0000-0002-5812-6621; C.E.B., 0000-0003-1565-7489

Received 29 March 2019; Accepted 7 August 2019

Development (2019) 146, dev178632. doi:10.1242/dev.178632

unappreciated, GFP expression was detected prior to injury in compact myocardium that is largely non-proliferative (Poss et al., 2002; Raya et al., 2003; Wills et al., 2008) by immunostaining with EGFP antibodies (Fig. 1A). We also detected expression by immunostaining after injury in compact and trabecular cardiomyocytes (Fig. 1B), both of which make contributions to regenerated muscle (Kikuchi et al., 2010; Pfefferli and Jaźwińska, 2017).

We used fluorescence-activated cell sorting (FACS) to isolate $EGFP^+$ cardiomyocytes from the apical halves of homeostatic and regenerating *Tg(gata4:EGFP)* hearts at 5 days post-amputation (dpa), a relatively early stage of cardiomyocyte proliferation (Poss et al., 2002) (Fig. 1C-E). RNA-seq followed by differential gene expression analysis identified 1041 upregulated and 994 downregulated (adjusted $P<0.05$) genes in proliferating cardiomyocytes compared with controls (Fig. 1F; Table S1). Gene ontology (GO) analysis in the upregulated subset of genes revealed over-represented functional categories that included cell cycle regulators, ECM components and remodelers, and numerous proteasome subunits (Fig. 1G; Fig. S1; Table S2). By contrast, the downregulated subset included sarcomere components, metabolic enzymes and modulators of higher-order cytoskeleton organization (Fig. 1G; Fig. S1; Table S2). These expression dynamics are consistent with previous studies demonstrating that mature cardiomyocytes detach from the actively remodeling ECM (Marro et al., 2016; Sánchez-Iranzo et al., 2018; Wang et al., 2013), disassemble their sarcomeres (Fan et al., 2015; Jopling et al., 2010) and decrease metabolic demands (Kikuchi et al., 2010; O'Meara et al., 2015; Wang et al., 2013) during heart regeneration. We validated our dataset by localizing highly induced transcripts in cardiac sections and observed injury-dependent signals in wound-edge cardiomyocytes in all cases (Fig. S2). Therefore, our system accurately captured the molecular hallmarks of zebrafish cardiomyocytes as they transition to a proliferative state.

To identify candidate regulators of these transcriptional dynamics, we examined our dataset for differential expression of chromatin regulators (Fig. 1H; Table S1). Notably, 5 dpa cardiomyocytes showed significant alterations in the expression of enzymes that catalyze H3K4 and H3K27 tri-methylation. Specifically, transcripts encoding Ezh2, the PRC2 methyltransferase that deposits H3K27me3 repressive marks (Simon and Kingston, 2013), were upregulated 2.8-fold, while transcripts encoding Kdm6b, which removes H3K27me3 (Black et al., 2012), were downregulated 2.4-fold (Table S2). Moreover, we observed a 2.0-fold downregulation of the Kmt2 methyltransferases that catalyze H3K4me3 (Black et al., 2012). Using double immunofluorescence on cardiac sections, we found that Ezh2 is upregulated by injury specifically in cardiomyocytes that are localized to the wound edge. Indeed, Ezh2 is highly expressed in the myocardial subpopulation that reinitiates expression of the embryonic form of cardiac myosin heavy chain (embCMHC) (Sallin et al., 2015) (Fig. 1I,J), upregulates EGFP in *Tg(gata4:GFP)* animals (Fig. S3) and gives rise to new cardiomyocytes in the regenerated tissue (Kikuchi et al., 2010). Ezh2 expression can also be observed in non-myocardial cells inhabiting the wound. These data demonstrate that injury-induced Ezh2 expression is a hallmark of proliferative cardiomyocytes that have repressed a subset of genes during zebrafish heart regeneration.

To identify the genomic loci showing dynamic methylation patterns, we performed chromatin immunoprecipitation followed by sequencing (ChIP-seq) on apical cardiomyocytes from uninjured and 5 dpa ventricles using H3K4me3- and H3K27me3-specific antibodies. We integrated our RNA-seq and ChIP-seq datasets to directly compare expression changes with histone methylation patterns. Specifically, expression levels of transcriptional start sites (TSSs) of genes that were differentially regulated were divided into significantly upregulated (upper panel, $n=1602$) or downregulated (lower panel, $n=1643$) categories (Fig. 1K; Table S3). ChIP-seq read densities were quantified within a ±2 kb window around each TSS to identify genes that also display robust changes in chromatin marks in response to injury (Table S3).

GO analysis of genes showing the highest changes (top 20%) in histone marks demonstrated clear enrichments for functions previously linked to the myocardial injury response (Fig. 1K; Table S4). For example, upregulated genes that gained the active H3K4me3 mark were enriched for cell cycle regulators (Fig. 1K, top green box; Table S4), whereas those that lost the repressive H3K27me3 mark were enriched for functions in protein degradation (Fig. 1K; bottom green box; Table S4). Upregulated genes that both gained H3K4me3 and lost H3K27me3 encoded proteins involved in ECM remodeling and cell cycle activity (Fig. 1K; far right dark green box; Tables S3 and S4), processes that are essential for myocardial renewal (González-Rosa et al., 2017; Vivien et al., 2016). Conversely, downregulated genes that gained H3K27me3 (Fig. 1K; top red box; Tables S3 and S4) or lost H3K4me3 (Fig. 1K; bottom red box; Tables S3 and S4), or both (Fig. 1K; far right dark red box; Tables S3 and S4), mostly encoded sarcomere and cytoskeletal components. Together, our integrated genome-wide analysis demonstrates that alterations in the histone code are associated with gene expression changes following cardiac injury. Moreover, our study identifies key structural genes as a target category for injury-induced H3K27me3 deposition in the regenerating myocardium.

Next, we investigated a functional requirement for H3K27me3-mediated gene silencing during zebrafish heart regeneration. To this end, we engineered a Cre-sensitive, heat shock-inducible transgenic strain that expresses a mutated version of histone 3 ($h3.3^{K27M}$) in which the lysine (K) at position 27 is mutated to a methionine (M) (Lewis et al., 2013; Venneti et al., 2013) (Fig. 2A). Importantly, $h3.3^{K27M}$ is not only insensitive to methylation, but also functions as a dominant negative by sequestering PRC2 (Bender et al., 2013). We recombined the *hsp70l:loxPmKateSTOPloxPh3.3*^{K27M} transgene specifically in cardiomyocytes during embryogenesis using the *cmlc2:creER*^{T2} driver strain (Kikuchi et al., 2010) (Fig. 2A) to generate *Tg(hsp70l:h3.3*^{K27M}*)*^{CM} animals (Fig. 2B). As a control, we analyzed *Tg(hsp70l:h3.3)* adults, which express wild-type *h3.3* ubiquitously in response to heat exposure (Fig. 2A). Immunostaining of cardiac sections with an H3K27me3-specific antibody demonstrated that heat shocking *Tg(hsp70l:h3.3*^{K27M}*)*^{CM} animals inhibits H3K27me3 specifically in cardiomyocytes compared with heat shocked *h3.3*-expressing (Fig. 2C-F) or non-transgenic controls (Fig. S4). By contrast, the same hearts did not show global changes in myocardial H3K27 acetylation (H3K27Ac; Fig. S5).

To determine whether H3K27me3 dynamics are required for zebrafish heart regeneration, we resected *Tg(hsp70l:h3.3*^{K27M}*)*^{CM} hearts, performed daily heat shocking for 2 months during the regenerative window (Fig. 2B), and examined cardiac sections immunostained with the muscle-specific tropomyosin (TPM) antibody at 60 dpa. We also quantified scar size in sections stained with Acid Fuschin-Orange G (AFOG). While control *Tg(hsp70l:h3.3)* animals that were injured, heat shocked and analyzed in parallel achieved robust myocardial regeneration (Fig. 2G) with little scarring (Fig. 2J; Fig. S6), *Tg(hsp70l:h3.3*^{K27M}*)*^{CM} hearts showed deficiencies in muscle renewal evidenced by gaps in the myocardial wall (Fig. 2H,I) with variable amounts of scar tissue (Fig. 2K,L; Fig. S6). These data demonstrate that H3K27me3 catalysis in cardiomyocytes is required for heart regeneration *in vivo*.

Development (2019) 146, dev178632. doi:10.1242/dev.178632

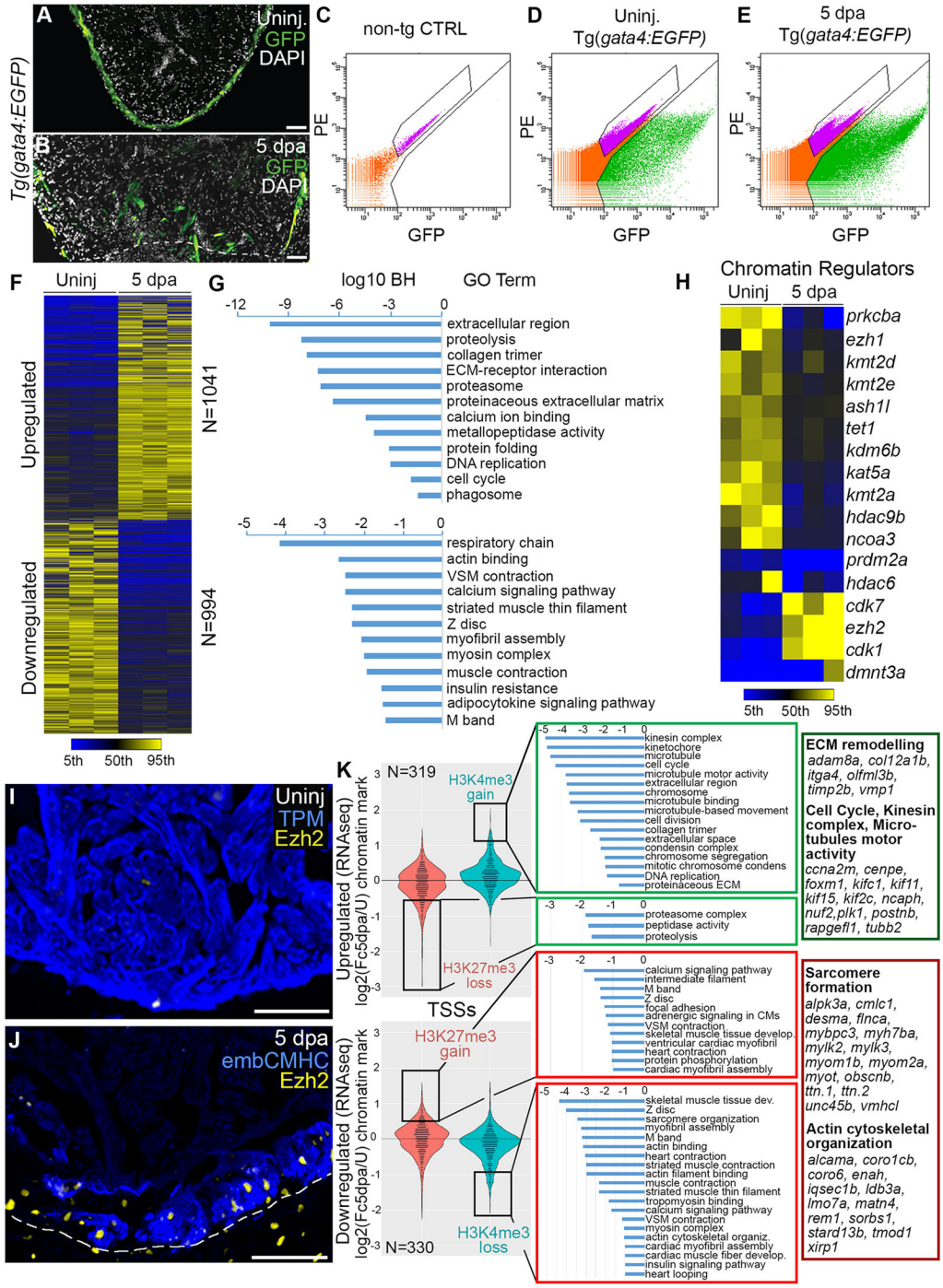

Fig. 1. H3K27me3 deposition is associated with reduced expression of genes encoding sarcomere and cytoskeletal components in proliferating cardiomyocytes during zebrafish heart regeneration. (A,B) Cardiac sections of uninjured (*n*=5) and 5 dpa (*n*=5) *Tg(gata4:EGFP)* ventricles immunostained for GFP (green) and counterstained with DAPI (white). (C-E) FACS analysis from single cell suspensions of pooled non-transgenic control (C), uninjured *Tg(gata4:EGFP)* (D) or 5 dpa *Tg(gata4:EGFP)* (E) ventricular apices with GFP fluorescence on the *x* axis and phycoerythrin (PE) on the *y* axis. Autofluorescence (gated pink dots) was distinguished from the GFP signal (gated green dots) based on the non-transgenic control FACS profile. The proportion of GFP^+ cardiomyocytes increased from 3.5% (D) to 9.3% (E) of the total cell population following injury. Cells in the GFP^+ gate were sorted and collected for RNA-seq. (F) Heat map depicting fold changes for all genes showing statistically significant differences between uninjured and 5 dpa GFP^+ cardiomyocytes ($P<0.05$). Three biological replicates are shown per cohort. (G) Significantly enriched gene ontology (GO) terms associated with upregulated and downregulated genes. (H) Heat map depicting significant fold changes of chromatin regulator genes in proliferating cardiomyocytes. (I) Representative section of an uninjured ventricle co-immunostained for tropomyosin (TPM, blue) and Ezh2 (yellow) (*n*=6 hearts). (J) Representative section of a 5 dpa ventricle co-immunostained for embryonic cardiac myosin heave chain (embCMHC, blue) and Ezh2 (yellow) (*n*=6 hearts). (K) ChIP-seq and RNA-seq data integration. RNA-seq isoform-level data were collapsed to obtain transcription start site (TSS)-specific expression levels, and TSSs displaying significant differential expression at 5 dpa were divided into either significantly upregulated (upper panel, *n*=1602) or downregulated (lower panel, *n*=1643) categories. Ratios of relative ChIP-seq read densities between 5 dpa and uninjured within a ±2 kb window around each TSS are represented in violin plots. Gene Ontology analysis was performed on the top and bottom 20% most-biased TSSs. Representative functional categories of genes possessing TSSs with both H3K4me3 and H3K27me3 dynamics are shown. Scale bars: 100 µm in A,B; 50 µm in I,J.

Development (2019) 146, dev178632. doi:10.1242/dev.178632

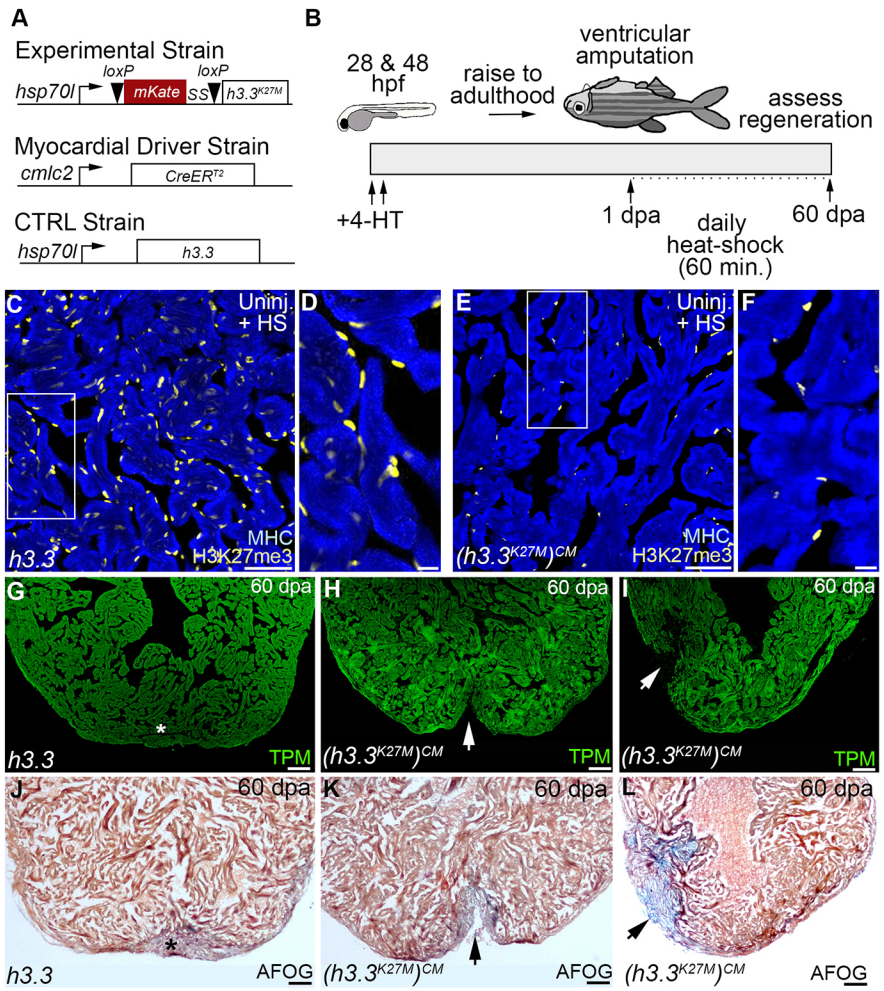

Fig. 2. Myocardial H3K27 tri-methylation is required for zebrafish heart regeneration *in vivo*. (A) Schematics depicting driver and inducible transgenes used for Cre/loxP-mediated myocardial-specific expression of *Tg(hsp70l:h3.3)* (wild-type control) or *Tg(hsp70l:h3.3^{K27M})^{CM}* (mutant) during the regenerative window. (B) Schematic depicting the experimental strategy for heart regeneration analyses. Double-transgenic embryos were exposed to 4-HT at 24 h post-fertilization (hpf) and 48 hpf to recombine the mutant transgene specifically in the myocardium. Zebrafish were raised to adulthood and their ventricles resected followed by a 24 h recovery period and daily 1 h heat-shocking for 60 days prior to analysis. (C-F) Sections of uninjured zebrafish ventricles co-immunostained for the cardiomyocyte marker, myosin heavy chain (blue) and H3K27me3 (yellow). Boxed regions in C and E are shown in D and F. Myocardial and non-myocardial cells displayed strong H3K27me3 signals in *Tg(hsp70l:h3.3)* hearts (C,D; *n*=5/5 hearts). By contrast, myocardial H3K27me3 signals failed to be detected in *Tg(hsp70l:h3.3^{K27M})^{CM}* hearts, whereas non-myocardial signals were preserved (E,F; *n*=5/5 hearts). (G-L) Representative cardiac sections from 60 dpa heat-shocked *Tg(hsp70l:h3.3)* control (G,J) and *Tg(hsp70l:h3.3^{K27M})^{CM}* (H,I,K,L) animals evaluated by immunofluorescence for the myocardial marker TPM (green; G-I) or AFOG staining (J-L). Whereas control animals robustly regenerated myocardium (asterisks in G,J; *n*=9/9 hearts), *Tg(hsp70l:h3.3^{K27M})^{CM}* hearts failed to regenerate new muscle (arrows in H and I; *n*=9/11) with either ventricular wall deficits (arrow in K; *n*=4/11) or apparent collagen deposits indicative of scarring (arrow in L; *n*=5/11). Scale bars: 50 µm in C, E; 10 µm in D,F; 100 µm in G-L.

We next sought to understand how impaired cardiomyocyte H3K27me3 deposition undermines heart regeneration. Using RT-qPCR, we evaluated ventricular apices from heat-shocked control and *Tg(hsp70l:h3.3^{K27M})^{CM}* hearts on 5 dpa for the expression of five genes encoding sarcomere components (*cmlc1*, *flnca*, *ttn.1*, *ttn.2* and *vmhcl*), the transcriptional repression of which during regeneration is associated with gains in H3K27me3 (Fig. 1F,K; Tables S3 and S4). *Tg(hsp70l:h3.3^{K27M})^{CM}* hearts expressed significantly higher levels of all five transcripts (Fig. 3A), demonstrating that H3K27me3 deposition contributes to their repression.

The induction of Ezh2 in wound-edge cardiomyocytes during regeneration (Fig. 1I,J) suggests that repressed genes would be similarly restricted to the wound edge. Using *in situ* hybridization, we localized expression of one of these transcripts, *vmhcl*, on cardiac sections from heat-shocked control hearts at 5 dpa. Indeed, we observed reduced expression of *vmhcl* specifically in wound-edge cardiomyocytes (Fig. 3B). By contrast, 5 dpa *Tg(hsp70l:h3.3^{K27M})^{CM}* hearts retained expression of *vmhcl* transcripts that extended to the wound edge (Fig. 3C), demonstrating their failure to respond to injury. To determine whether *Tg(hsp70l:h3.3^{K27M})^{CM}*-expressing cardiomyocytes are capable of re-initiating embCMHC (Sallin et al., 2015) expression, we co-stained cardiac sections for embCMHC and tropomyosin (TPM) at 10 dpa when levels are high. Unlike control hearts that showed robust embCMHC expression in wound area TPM$^+$ cardiomyocytes (Fig. 3D,F), *Tg(hsp70l:h3.3^{K27M})^{CM}* ventricles showed reduced expression (Fig. 3E,F). Together, our molecular analyses suggest that diminished H3K27me3 modifications in wound edge cardiomyocytes results in a failure to downregulate sarcomere gene expression and the retention of a more mature myocardial fate.

To analyze the cellular consequences of this failed transcriptional repression, we monitored sarcomere structure at 10 dpa in wound edge cardiomyocytes by immunostaining cardiac sections from heat-shocked control and *Tg(hsp70l:h3.3^{K27M})^{CM}* hearts for TPM to visualize the characteristic striated pattern. Although the majority of wound edge cardiomyocytes expressed TPM in control hearts, these cells were largely devoid of striations (Fig. 3G,H). By contrast, prominent striations were visible in *Tg(hsp70l:h3.3^{K27M})^{CM}* hearts (Fig. 3I,J). We quantified this phenotype by dissociating 5 dpa ventricular apices into single cells, double immunostaining for embCMHC and TPM, and determining the percentages of embCMHC$^+$ cardiomyocytes with intact or disassembled sarcomeres (Fig. 3K-Q). In control hearts, 83% of embCMHC$^+$ cardiomyocytes showed evidence of disrupted sarcomere structure compared with only 38% in mutant hearts. These data demonstrate that sarcomere break down is compromised by decreased H3K27me3 deposition following injury.

We next tested whether impaired sarcomere disassembly in wound edge cardiomyocytes undermines cell cycle re-entry by immunostaining cardiac sections from heat-shocked control and *Tg(hsp70l:h3.3^{K27M})^{CM}* hearts for PCNA to mark cells undergoing DNA replication and Mef2 to identify cardiomyocyte nuclei. Surprisingly, the proportion of PCNA$^+$ cardiomyocytes at the wound edge was indistinguishable between experimental groups

Development (2019) 146, dev178632. doi:10.1242/dev.178632

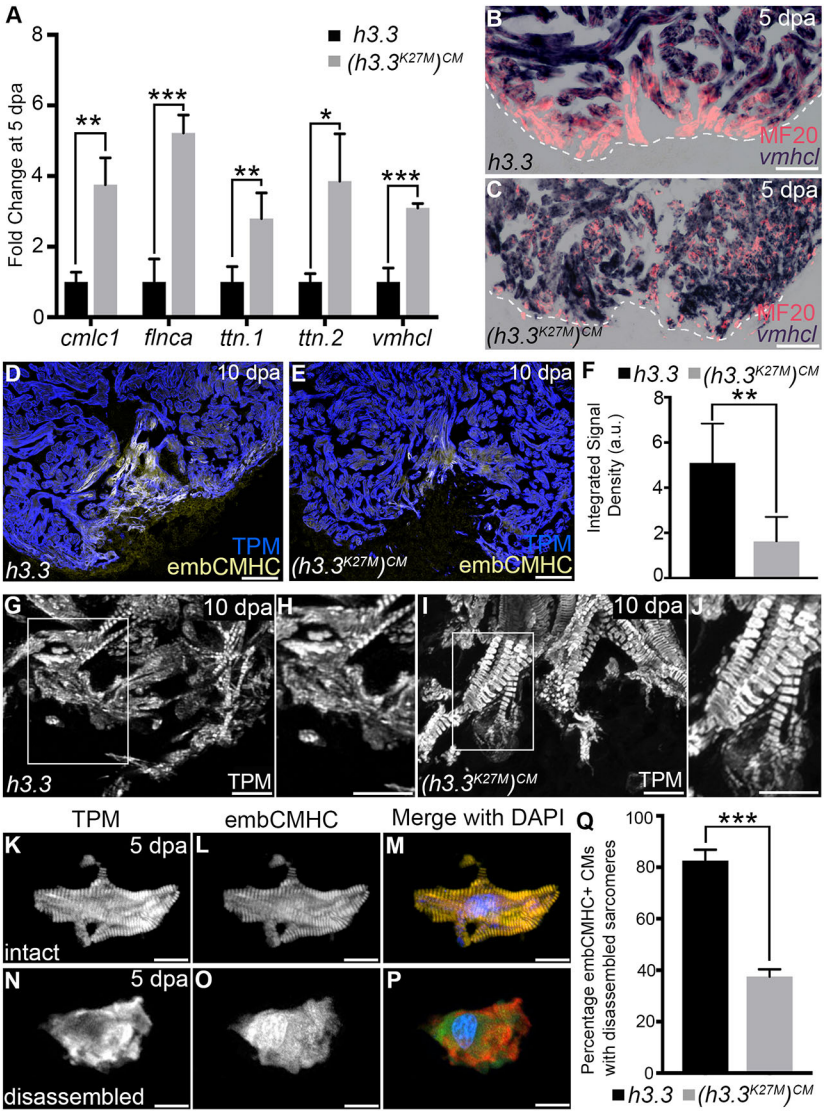

Fig. 3. H3K27me3 deposition is required for sarcomere disassembly in wound edge cardiomyocytes. (A) Bar graph showing relative levels of sarcomeric transcripts in *Tg(hsp70l:h3.3)* and *Tg(hsp70l:h3.3^{K27M})^{CM}* wound edge samples at 5 dpa, as measured by quantitative PCR (*n*=3 biological replicates for each cohort). Data are mean±s.d. **P*<0.05; ***P*<0.01; ****P*<0.001. (B,C) Section *in situ* hybridization for ventricular myosin (*vmhcl*) expression (blue) and antibody staining for myosin heavy chain (red). Control *Tg(hsp70l:h3.3)* hearts (B; *n*=6/6), but not *Tg(hsp70l:h3.3^{K27M})^{CM}* hearts (C; *n*=5/5), exhibit reduced *vmhcl* expression in wound edge myocardium at 5 dpa. (D,E) Representative *Tg(hsp70l:h3.3)* (D) or *Tg(hsp70l:h3.3^{K27M})^{CM}* (E) cardiac sections co-immunostained for tropomyosin (TPM; blue) and embCMHC (yellow). *Tg(hsp70l:h3.3^{K27M})^{CM}* hearts showed relatively lower embCMHC signals at the wound edge compared with *Tg(hsp70l:h3.3)* hearts (*n*=8/8 and 11/11 hearts, respectively). (F) Bar graph showing the integrated signal densities of embCMHC in arbitrary units in *Tg(hsp70l:h3.3)* and *Tg(hsp70l:h3.3^{K27M})^{CM}* hearts at 10 dpa. (G-J) Wound edge regions in cardiac sections immunostained for tropomyosin (TPM) at 10 dpa in *Tg(hsp70l:h3.3)* or *Tg(hsp70l:h3.3^{K27M})^{CM}* hearts. Boxed regions in G and I are shown in H and J, respectively. Although wound edge cardiomyocytes show dissociated sarcomeres in *Tg(hsp70l:h3.3)* animals (*n*=5/5), sarcomere structure appears preserved in *Tg(hsp70l:h3.3^{K27M})^{CM}* animals (*n*=4/6). (K-P) Split channel (K,L,N,O) or merged (M,P) confocal scans of dissociated cardiomyocytes immunostained for tropomyosin (TPM; red) and embryonic cardiac myosin heavy chain (embCMHC; green), and counterstained with DAPI (blue) to visualize sarcomere integrity in injury-responsive cardiomyocytes. (Q) The percentage of embCMHC^{+} cardiomyocytes with partially disassembled sarcomeres as shown in N-P in *Tg(hsp70l:h3.3)* (*n*=57 embCMHC+ CMs derived from nine apices) and *Tg(hsp70l:h3.3^{K27M})^{CM}* (*n*=77 embCMHC+ CMs derived from nine apices) hearts. Data are mean±s.d. **P*<0.05; ***P*<0.01; ****P*<0.001. *P*-values were calculated using unpaired two-tailed Student's *t*-test. Scale bars: 100 µm in B-E; 10 µm in G-P.

(Fig. 4A-E), a finding that we confirmed by quantifying BrdU^{+} cardiomyocytes at 14 dpa after a single IP injection of the thymidine analog at 5 dpa (Fig. 4F). Because mitosis and cytokinesis cannot be inferred from PCNA or BrdU incorporation, we analyzed cardiomyocytes in *Tg(hsp70l:h3.3^{K27M})^{CM}* hearts for failed nuclear or cellular division. Specifically, an inability to complete mitosis would result in mononucleated cardiomyocytes (Fig. 4G) with doubled DNA content (ploidy), whereas impaired cytokinesis would lead to cardiomyocyte binucleation (Fig. 4H). By analyzing ploidy in mononucleated wound edge cardiomyocytes from 14 dpa ventricles, we observed no significant difference between cohorts (Fig. 4I), demonstrating that mitosis is unaffected by H3K27me3 dynamics. However, the percentages of binucleated cardiomyocytes in the same samples were significantly increased from <2% in controls to ~10% in *Tg(hsp70l:h3.3^{K27M})^{CM}* hearts (Fig. 4J). Although this increase in binucleation could be due to aberrant cell fusions, the more plausible mechanism is an increase in cytokinesis failures that might be attributed to abnormally persistant sarcomere and cytoskeletal structure.

In addition, we noticed that myocardial nuclear density appeared increased in *Tg(hsp70l:h3.3^{K27M})^{CM}* hearts, suggesting a defect in cardiomyocyte wound infiltration. Indeed, mutant hearts contained 1.5-fold more myocardial nuclei within 200 µm of the wound edge compared with controls (Fig. 4K-M). As a reciprocal approach, we quantified the number of TPM^{+} cardiomyocytes within the wound region. This domain, which is initially devoid of cardiomyocytes, stains more prominently with phalloidin than the surrounding myocardium (Fig. 4N), and was colonized by large numbers of TPM^{+} cardiomyocytes in control hearts by 10 dpa (Fig. 4N-P,T), whereas the wound region of *Tg(hspl:h3.3^{K27M})^{CM}* hearts showed a fourfold reduction (Fig. 4Q-T). Overall, our results demonstrate that H3K27me3 catalysis is required for cardiomyocytes to infiltrate the wound. While physical constraints on cell movement caused by sarcomere maintenance might underlie this deficiency, increased cell-cell contacts and decreased ECM remodeling could also contribute to this phenotype.

Our integrated genome-wide analyses support a model in which cardiac injury stimulates chromatin remodeling in wound edge cardiomyocytes that leads to targeted H3K27me3-mediated repression of key structural genes. The transcriptional profile we observed in zebrafish cardiomyocytes on 5 dpa shows a striking resemblance to that observed in neonatal mouse cardiomyocytes following injury (Natarajan et al., 2018; O'Meara et al., 2015), highlighting shared gene expression signatures between species. Specifically, injury-responsive cardiomyocytes in both zebrafish and mouse reduce transcripts encoding sarcomere components,

Development (2019) 146, dev178632. doi:10.1242/dev.178632

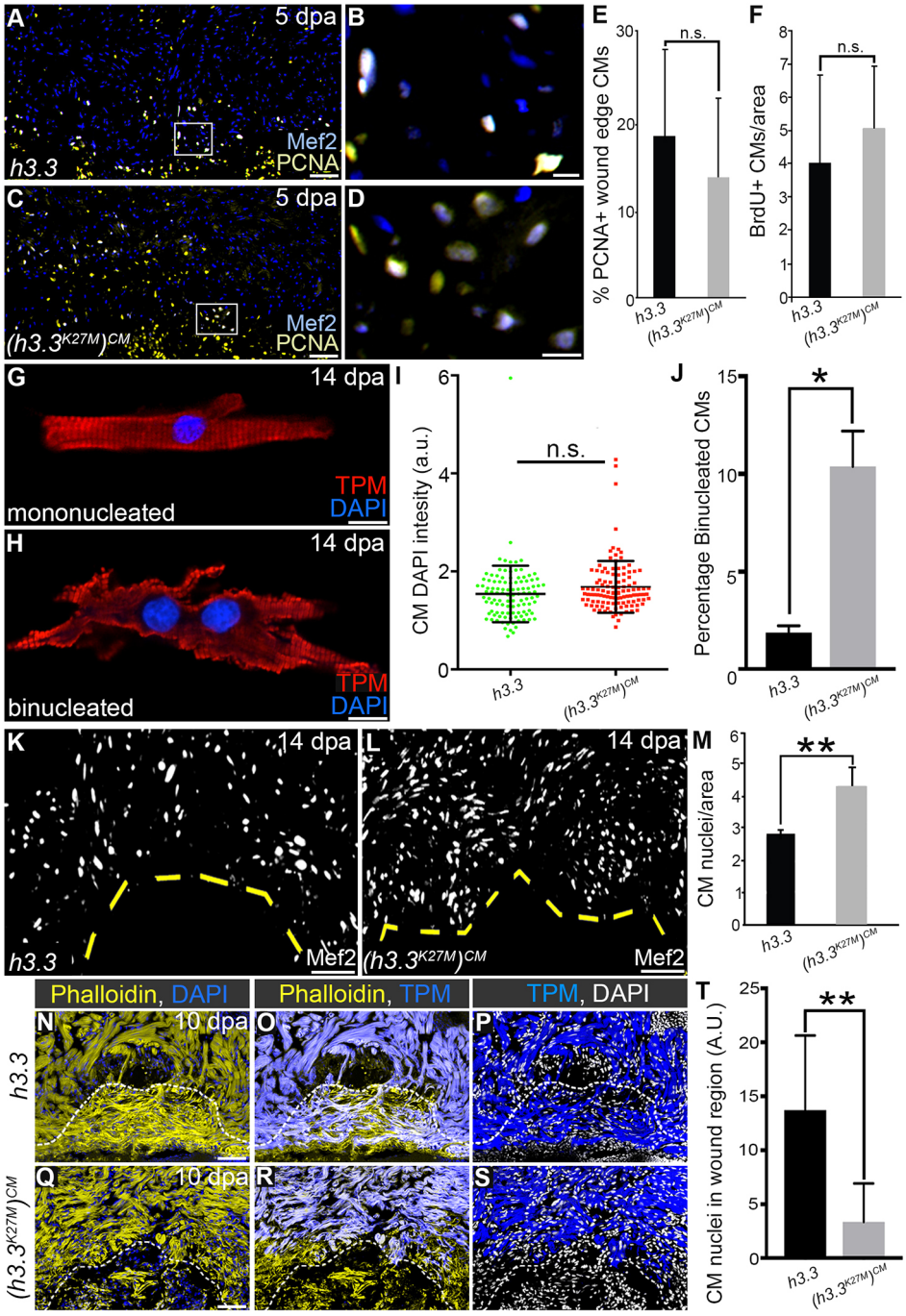

Fig. 4. Injury-induced H3K27me3 deposition is required for cardiomyocyte cytokinesis and wound invasion during zebrafish heart regeneration. (A-D) Representative cardiac sections from heat-shocked *Tg(hsp70l:h3.3)* and *Tg(hsp70l:h3.3^{K27M})^{CM}* animals at 5 dpa. Sections were double immunostained to identify cardiomyocyte nuclei (Mef2^{+}; blue) and nuclei undergoing DNA replication (PCNA^{+}; yellow). Boxed regions in A and C are shown at higher magnification in B and D, respectively. (E) The percentages of myocardial nuclei undergoing DNA replication near the wound edge were quantified and reported as mean proliferation indices (*n*=5 hearts for each cohort). Data are mean±s.d. n.s., not significant. (F) The percentages of myocardial nuclei that incorporated BrdU between 5 and 14 dpa near the wound edge were quantified and reported as mean proliferation indices [*n*=8 *Tg(hsp70l:h3.3)*; *n*=5 *Tg(hsp70l:h3.3^{K27M})^{CM}*]. (G,H) Fluorescent images of cardiomyocytes immunostained for tropomyosin (TPM) and counterstained with DAPI from dissociated *Tg(hsp70l:h3.3)* or *Tg(hsp70l:h3.3^{K27M})^{CM}* ventricles following heat shock at 5 dpa. (I) The distribution of DNA content per nucleus in dissociated *Tg(hsp70l:h3.3)* (*n*=110 cells from 12 hearts) or *Tg(hsp70l:h3.3^{K27M})^{CM}* (*n*=127 cells from 12 hearts) cardiomyocytes (as shown in G,H) based on DAPI fluorescence intensity. (J) The percentage of binucleated cardiomyocytes in *Tg(hsp70l:h3.3)* or *Tg(hsp70l:h3.3^{K27M})^{CM}* ventricular dissociations. (K,L) Representative cardiac sections from heat-shocked *Tg(hsp70l:h3.3)* (*n*=3 hearts) and *Tg(hsp70l:h3.3^{K27M})^{CM}* (*n*=5 hearts) animals at 14 dpa. Sections were immunostained to identify cardiomyocyte nuclei (Mef2). (M) Graph quantifying the wound edge CM nuclear density (CM nuclei per 200 µm). (N-S) Representative cardiac sections from heat-shocked *Tg(hsp70l:h3.3)* (*n*=10 hearts) and *Tg(hsp70l:h3.3^{K27M})^{CM}* (*n*=5 hearts) animals at 10 dpa immunostained for tropomyosin (TPM, blue) and counterstained with DAPI to highlight nuclei and phalloidin to visualize the actin cytoskeleton in cells localized within the wound region and spared area. (T) Quantification of CM nuclei within the wound region in heat-shocked *Tg(hsp70l:h3.3)* and *Tg(hsp70l:h3.3^{K27M})^{CM}* hearts. Data are mean±s.d. *P<0.05; **P<0.01; n.s., not significant. *P*-values were calculated using unpaired two-tailed Student's *t*-test. Scale bars: 50 µm in A,C,K,L,N-S; 10 µm in B,D,G,H.

Development (2019) 146, dev178632. doi:10.1242/dev.178632

cytoskeletal actin and metabolism-related factors, while increasing expression of proteases and cell cycle components. Therefore, we speculate that conserved mechanisms promote successful regenerative outcomes between species. Because maintenance of sarcomere structure is likely a major barrier for heart regeneration in adult mammals, myocardial PRC2 activation might be leveraged to stimulate cardiomyocyte proliferation in the human heart after acute insult for therapeutic benefit.

MATERIALS AND METHODS

Experimental model and subject details

Zebrafish embryos, larvae and adults were produced, grown and maintained according to animal protocols approved by the Massachusetts General Hospital and Boston Children's Hospital Institutional Animal Care and Use Committee. For adult zebrafish, approximately equal sex ratios of animals ranging from 6 to 36 months of age were used. Adult density was maintained at ∼4 fish per liter. Published zebrafish strains used in this study include: *Tg(gata4:GFP)*^{ae1} (Kikuchi et al., 2010) and *Tg(cmlc2:CreER*^{T2}*)*^{pd10} (Kikuchi et al., 2010). Details of the construction of new transgenic lines are described below.

Construction of *Tg(hsp70l:h3.3)*

To generate the *Tg(hsp70l:h3.3)* line, Gateway technology (Life Sciences) was used. A middle clone was engineered that contains the zebrafish *h3f3a* cDNA. This clone was recombined with the previously described 5′ (*p5E-hsp70l*) and 3′ (*p3E-polyA*) entry clones (Kwan et al., 2007), and a Tol2 flanked destination vector, pDest-Tol2AB2 (Zhou et al., 2011), that carries a lens-specific promoter upstream of the Cerulean fluorescent protein. This transgene was injected into one-cell stage zebrafish embryos with Tol2 transposase mRNA to aid in transgenesis.

Construction of *Tg(hsp70l:loxP-mKate2-SS-loxP-h3.3*^{K27M}*)*

To generate the *Tg(hsp70l:loxP-mKate2-SS-loxP- h3.3*^{K27M}*)* line, lysine 27 was mutated to methionine in the zebrafish *h3f3a* Gateway middle clone (see above) by PCR using mismatched primers (see Table S5 for primer sequences). This middle clone was recombined with the 5′ (*p5E-hsp70l*) and 3′ (*p3E-polyA*) entry clones (Kwan et al., 2007), and a Tol2 flanked destination vector, pDest-Tol2AB2 (Zhou et al., 2011), that carries a lens-specific promoter upstream of the Cerulean fluorescent protein. This transgene was injected into one-cell stage zebrafish embryos with Tol2 transposase mRNA to aid in transgenesis.

Zebrafish cardiac resections

Apical resections were performed on male and female adult zebrafish between 6-36 months of age as previously described (Poss et al., 2002). Briefly, fish were anesthetized in tricaine, placed ventral side up on a slotted sponge, and opened surgically to expose the apex of the ventricle. Approximately 20% of the apex region was amputated with iridectomy scissors. Following the surgery, zebrafish were placed in their tanks and revived by gently moving water over their gills with a plastic Pasteur pipet.

4-HT and heat-shock administration

To induce CreER^{T2}-mediated transgene recombination, zebrafish embryos were exposed to 10 µM 4-hydoxy-tamoxifen (4-HT, Sigma) for 1 h at 24 and 48 h post-fertilization. Treated animals were washed in E3, raised to adulthood, and used in experiments described below. After ventricular resection surgery and overnight recovery, zebrafish were placed on an automated heat shock rack that exposed them to daily temperature elevations from 28 to 39°C, as previously described (Zhao et al., 2014).

Quantitative polymerase chain reaction (qPCR)

The fibrin clot was cleared from ventricles dissected from *Tg(hsp70l:h3.3)* or *Tg(hsp70l:h3.3K27M)* adults at 5 dpa and the apical one-third of a single ventricle was used per biological replicate. Three biological replicates were analyzed. Tissue was homogenized using a pestle and processed with RNAeasy (Qiagen) to purify total RNA. RNA was transcribed to cDNA using Superscript III First-Strand Synthesis System (Life Technologies). Quantitative PCR analysis was performed using Fast SYBR Green Master Mix (Life Technologies) and an Applied Biosystems 7500 Real-Time PCR System (Life Technologies) according to the manufacturer's instructions. The 2−ΔΔCT method (Livak and Schmittgen, 2001) was used to measure differential expression levels after normalization to *actb2* (see Table S5 for primer sequences.)

Isolation of cardiomyocytes

Hearts were removed and cleared of injury tissue in a petri dish containing PBS. The apical one-third of the ventricle was excised and dissociated into single cell suspensions using the mouse neonatal heart dissociation kit (Miltenyi Biotec).

For isolation of *gata4:GFP*$^{+}$ cells for RNAseq analysis, GFP^{+} cells were sorted on a BD FACSAria instrument at the Harvard Stem Cell Institute Flow Cytometry Core into lysis buffer (RNeasy micro kit, Qiagen). For ChIP applications, cells were fixed for 30 min at 37°C using a final concentration of 1% methanol-free formaldehyde (Life Technologies, 28908) and strained through 10 µm nylon filters (Spectrum Labs) to enrich the cardiomyocyte population. The nylon strainers were attached to 15 ml conical tubes that were pierced to allow attachment to a vacuum tap. Light vacuum was applied to drain the liquid while cell suspensions were gradually applied to the strainer. The mesh and associated cells were transferred to a 1 ml tube and processed (cell lysis and DNA shearing) as previously described (Busby et al., 2016). The mesh was then removed using forceps. The chromatin immunoprecipitation (ChIP) and library construction were performed as described previously (Busby et al., 2016).

For cell spreads, dissociated cells were fixed using a final concentration of 4% paraformaldehyde (Thermo Fisher Scientific) for 30 min and washed with PBS. Drops of cell suspension were applied to histological glass slides and allowed to dry for 30 min at 37°C, washed in PBS and immunostained.

RNA-seq library construction

RNA integrity and concentration were determined on a Fragment Analyzer (Advanced Analytical). cDNA samples were generated using the Ovation low input v2 kit (Nugen) according to the manufacturer's recommendations. The resulting cDNA samples were then end-repaired and adaptor-ligated using the SPRI-works Fragment Library System I (Beckman Coulter Genomics) and indexed during amplification. Libraries were quantified using the Fragment Analyzer (Advanced Analytical) and qPCR before being loaded for paired-end sequencing 2×40 nt using the Illumina HiSeq 2000.

RNA-seq analysis

Reads from three replicates of uninjured ('uninjured') and 5 days post injury ('5 dpa') heart samples were aligned against the GRCz10 genome assembly of the Zebrafish, ENSEMBL 89 annotation using STAR versus 2.5.3a in paired-end mode with parameters –runThreadN 16 –runMode alignReads –outFilterType BySJout –outFilterMultimapNmax 20 –alignSJoverhangMin 8 –alignSJDBoverhangMin 1 –outFilterMismatchNmax 999 –alignIntronMin 10 –alignIntronMax 1000000 –alignMatesGapMax 1000000 –outSAMtype BAM SortedByCoordinate –quantMode TranscriptomeSAM. The resulting Aligned.toTranscriptome.out.bam files were post-processed using RSEM v. 1.3.0 using following flags –paired-end –calc-ci –alignments -p 8 –forward-prob 0. Posterior mean estimates of counts, RPKM and TPM were retrieved for each gene in each sample.

Differential expression analysis between uninjured and 5 dpa samples was performed using DESeq2 (Love et al., 2014) in the R statistical environment (v. 3.3.3) on protein-coding genes (according to ENSEMBL's biotype assignments). Genes with a Benjamini-Hochberg adjusted *P*-value for multiple comparison<0.1 were retained and their log-transformed RPKM values were quantile-normalized using the normalize.quantile function from the preprocessCore R package, magnitude normalized by row and displayed as heat maps in Spotfire (Tibco); genes were clustered by single-linkage clustering using correlation as a distance metric and normalization by standard deviation. Gene ontology analysis was performed in the DAVID 6.8 online statistical environment, on genes up- or downregulated in 5 dpa samples, using as a background all genes with baseMean>0 from the DESeq2 output based on their ENSEMBL identifiers.

Development (2019) 146, dev178632. doi:10.1242/dev.178632

ChIP-seq

Genome-wide localization of histone modifications H3K4me3 and H3K27me3 was determined by chromatin immunoprecipitation from fixed cell pellets (see Isolation of cardiomyocytes) followed by high-throughput sequencing. The following monoclonal antibodies were used: Cell Signaling C42D8 (H3K4me3) and C36B11 (H3K27me3). For detailed methods, see Busby et al. (2016).

ChIP-seq analysis

ChIP-seq reads were obtained in triplicate from uninjured, 5 dpa and a whole-cell extract sample [WCE, all samples sequenced at the Broad Institute Genomic Platform using Nextseq 500 with paired end (PE) reads] as aligned reads against the danRer7 genome assembly (bwa v. :0.5.9-tpx; bwa aln -q 5 -l 32 -k 2 out1.sai fastq_1 file; bwa aln -q 5 -l 32 -k 2 out2.sai fastq_2 file; bwa sampe -T -P -f out_sam_paired.sam Danio_rerio.fasta out1.sai out2.sai fastq_1 _fastq_2). Bam files from H3K4me3-ChIP were sorted by read names and converted into fastq files using bedtools v 2.26.0 bamtofastq in paired-end mode, and mapped to the GRCz10 Zebrafish genome assembly using bwa v. 0.7.12 with the same above-mentioned parameters (Li and Durbin, 2009). For H3K27me3 data, quality scores of bam files were adjusted using the CleanSam utility version 2.18.11, and files were converted to fastq and aligned against the GRCz10 Zebrafish genome assembly using bowtie2 v. 2.3.2 with default parameters, and -p 8. For all GRCz10-aligned files, mapped reads were marked with PICARD v. 2.8.1 MarkDuplicates function with parameters

MAX_SEQUENCES_FOR_DISK_READ_ENDS_MAP=50000
MAX_FILE_HANDLES_FOR_READ_ENDS_MAP=8000
SORTING_COLLECTION_SIZE_RATIO=0.25
REMOVE_SEQUENCING_DUPLICATES=false
TAGGING_POLICY=DontTag REMOVE_DUPLICATES=false
ASSUME_SORTED=false
DUPLICATE_SCORING_STRATEGY=SUM_OF_BASE_QUALITIES
PROGRAM_RECORD_ID=MarkDuplicates PROGRAM_GROUP_
NAME=MarkDuplicates
READ_NAME_REGEX=<optimized capture of last three ':' separated
fields as numeric values>
OPTICAL_DUPLICATE_PIXEL_DISTANCE=100 VERBOSITY=
INFO QUIET=false
VALIDATION_STRINGENCY=STRICT COMPRESSION_LEVEL=5
MAX_RECORDS_IN_RAM=500000 CREATE_INDEX=false
CREATE_MD5_FILE=false
GA4GH_CLIENT_SECRETS=client_secrets.json PN:MarkDuplicates.

H3K27me3 bam files were sorted and filtered with samtools to exclude sam flags 1796.

Integration of ChIP-seq and RNA-seq output

The resulting bam files were used to quantify read counts within 4 kb windows centered on annotated transcription start sites (TSSs; i.e. TSSs ±2 kb) with bedtools v. 2.26.0 (Quinlan and Hall, 2010) multicov (based on ENSEMBL release 89). Isoform-level transcriptional expression was retrieved from the RSEM pme output and read count matrices were obtained by summing isoforms that shared a TSS. Differential isoform expression was estimated with DESeq2 to obtain log2 fold-change data and significance levels (*P*-values) between uninjured and 5 dpa samples, and TSS were split between significantly up- or downregulated categories at 5 dpa. TSSs upstream of genes with adjusted *P*-values<0.1 in bulk RNA-seq differential expression analysis and with TSS-specific differential expression (assessed by an adjusted *P*-value<0.2) were retrieved for downstream analysis. For each TSS, H3K4me3- or H3K27me3-associated read densities were calculated in a ±2 kb window and DESeq2-based log2 fold-changes of such ratio between uninjured and 5 dpa samples were used to rank up- and downregulated TSSs independently. TSSs falling within the top and bottom 20% of the distribution of biases in chromatin marks were retrieved and corresponding gene lists were submitted to Gene Ontology analysis in the DAVID Bioinformatics environment 6.8 (Huang et al., 2009a,b), using the set of differentially regulated genes as a background for each chromatin mark independently. Finally, sets of significantly upregulated TSS that displayed both gains in H3K4me3 and losses of H3K27me3 were identified, and the resulting gene lists were inspected for functional enrichment/GO analysis. The reciprocal analysis was carried out for downregulated genes with gains in H3K27me3 and losses of H3K4me3.

Histology

Histological sectioning and immunohistochemistry were performed as previously described (Zhao et al., 2014). All antibody staining was performed on 10 µm cryosections following antigen retrieval (citrate buffer pH 6.0), except when phalloidin staining was also performed. The following antibodies were used: GFP (Life Technologies, A11122, 1:500); myosin heavy chain (Developmental Studies Hybridoma Bank, MF20, 1:50); embCMHC (Developmental Studies Hybridoma Bank, N2.261, 1:50); PCNA (Sigma, WH0005111M2, 1:250); Mef2 (Santa Cruz sc-313, 1:75); histone 3 tri-methyl K27 (Cell Signaling, C36B11, 1:100); Ezh2 (Cell Signaling, D2C9, 1:100); and BrdU (Abcam, ab6326, 1:50). Phalloidin staining (Life Technologies, A34055) was performed for 1 h at 1:40 dilution. Acid Fuchsin-Orange G (AFOG) staining and quantification of scar tissue was performed similarly to previous descriptions (Zhao et al., 2014) Briefly, an AFOG-stained representative section from the middle of each injury area was imaged as detailed below. Whole ventricular area and scar area were measured using ImageJ software. The scar area was normalized to the whole ventricular area to calculate the percentage of scar size in each heart.

Imaging

Histological sections were imaged on a Nikon Eclipse 80i compound microscope and Retiga 200R CCD digital camera (QImaging) or Excelis HDS Accu-Scope imaging system. Confocal imaging was performed on a Nikon A1 confocal microscope.

Proliferation and density analysis

Cardiomyocyte proliferation was determined by co-staining with Mef2 and PCNA or BrdU antibodies and counting the proportions of PCNA/BrdU-positive, Mef2-positive nuclei out of total Mef2-positive cells in the proximity of the wound. BrdU was administered by a single 25 µl intraperitoneal injection of 8 mg/ml BrdU (Sigma B5002) dissolved in PBS at 5 dpa. The ventricles were recovered and processed at 14 dpa.

In situ hybridization

Cryosections (10 µm) were incubated with 20 µg/ml proteinase K solution for 10 min followed by post-fixation in 4% paraformaldehyde and HCl treatment (0.2 M for 15 min). Sections were then pre-incubated with 50% formamide+total RNA hybridization solution at 65°C for 1 h followed by overnight incubation with hybridization solution+DIG-labeled RNA probes at 65°C. Bound probes were detected using alkaline phosphatase-conjugated anti-digoxigenin antibodies (Sigma-Aldrich, 11093274910) and staining using NBT/BCIP solution (Roche). For primer sequences used to generate probes, see Table S5.

Cardiomyocyte nucleation and ploidy analysis

Cardiomyocyte nucleation was scored manually using cell spreads stained for tropomyosin, embCMHC and DAPI. DNA content was determined by quantifying the integrated nuclear density of cells stained with the DNA dye DAPI.

Cardiomyocyte nuclei per area in the wound

Histological sections (10 µm) from 14 dpa hearts that were heat-shocked to induce either wild-type *h3.3* or $h3.3^{K27M}$ were immunostained for myosin heavy chain and Mef2. Cardiomyocyte nuclear density in the regenerating myocardium was quantified using the ImageJ suite by measuring $Mef2^{+}$ nuclei counts as a function of area.

Statistical analysis

P-values were calculated using unpaired two-tailed Student's *t*-test. Chi-square was used to calculate significance of differences between normal distributions of RNA expression data (Microsoft Excel, GraphPad Prism 7).

Acknowledgements
We thank K. Poss for providing *Tg(gata4:EGFP)* and *Tg(cmlc2:CreER^{T2})* zebrafish, and the Harvard Stem Cell Institute FACS core for technical assistance.

Competing interests
The authors declare no competing or financial interests.

Author contributions
Conceptualization: R.B.-Y., C.G.B., C.E.B.; Methodology: R.B.-Y., V.L.B., M.B., Y.Q., S.S.L., A.G., L.A.B., C.G.B., C.E.B.; Formal analysis: R.B.-Y., V.L.B., L.A.B., C.G.B., C.E.B.; Investigation: R.B.-Y., L.A.B., C.G.B., C.E.B.; Writing - original draft: L.A.B., C.G.B., C.E.B.; Writing - review & editing: R.B.-Y., V.L.B., A.G., L.A.B, C.G.B., C.E.B.; Supervision: A.G., L.A.B., C.G.B., C.E.B.; Project administration: C.G.B., C.E.B.; Funding acquisition: C.G.B., C.E.B..

Funding
R.B.-Y. was supported by a European Molecular Biology Organization long-term fellowship (LTF 119-2012). Work by V.L.B., S.S.L. and L.A.B. was supported by a National Cancer Institute award P30-CA14051 in addition to an American Heart Association grant (15GRNT25670044 to L.A.B.) and a National Institutes of Health grant (1-R01-HL140471-01 to L.A.B.). A.G. was supported by the Broad Institute Scientific Projects to Accelerate Research and Collaboration program. This work was supported by National Institutes of Health grants R01 HL127067 to C.G.B. and C.E.B., and R35 HL135831 to C.E.B.; and by a d'Arbeloff Massachusetts General Hospital Research Scholar Award to C.E.B. Deposited in PMC for release after 12 months.

Data availability
The ChIP-Seq and RNA-Seq raw and processed data have been deposited in the GEO under accession numbers GSE96928 and GSE96929, respectively.

Supplementary information
Supplementary information available online at
http://dev.biologists.org/lookup/doi/10.1242/dev.178632.supplemental

References

Ahmed, A., Wang, T. and Delgado-Olguin, P. (2018). Ezh2 is not required for cardiac regeneration in neonatal mice. *PLoS ONE* **13**, e0192238. doi:10.1371/journal.pone.0192238

Ahuja, P., Perriard, E., Perriard, J.-C. and Ehler, E. (2004). Sequential myofibrillar breakdown accompanies mitotic division of mammalian cardiomyocytes. *J. Cell. Sci.* **117**, 3295-3306. doi:10.1242/jcs.01159

Ai, S., Yu, X., Li, Y., Peng, Y., Li, C., Yue, Y., Tao, G., Li, C.-Y., Pu, W. T. and He, A. (2017). Divergent requirements for EZH1 in heart development versus regeneration. *Circ. Res.* **121**, 106-112. doi:10.1161/CIRCRESAHA.117.311212

Bassat, E., Mutlak, Y. E., Genzelinakh, A., Shadrin, I. Y., Baruch Umansky, K., Yifa, O., Kain, D., Rajchman, D., Leach, J., Riabov Bassat, D. et al. (2017). The extracellular matrix protein agrin promotes heart regeneration in mice. *Nature* **547**, 179-184. doi:10.1038/nature22978

Bender, S., Tang, Y., Lindroth, A. M., Hovestadt, V., Jones, D. T. W., Kool, M., Zapatka, M., Northcott, P. A., Sturm, D., Wang, W. et al. (2013). Reduced H3K27me3 and DNA hypomethylation are major drivers of gene expression in K27M mutant pediatric high-grade gliomas. *Cancer Cell* **24**, 660-672. doi:10.1016/j.ccr.2013.10.006

Black, J. C., Van Rechem, C. and Whetstine, J. R. (2012). Histone lysine methylation dynamics: establishment, regulation, and biological impact. *Mol. Cell* **48**, 491-507. doi:10.1016/j.molcel.2012.11.006

Busby, M., Xue, C., Li, C., Farjoun, Y., Gienger, E., Yofe, I., Gladden, A., Epstein, C. B., Cornett, E. M., Rothbart, S. B. et al. (2016). Systematic comparison of monoclonal versus polyclonal antibodies for mapping histone modifications by ChIP-seq. *Epigenet. Chromatin* **9**, 49. doi:10.1186/s13072-016-0100-6

Fan, X., Hughes, B. G., Ali, M. A. M., Cho, W. J., Lopez, W. and Schulz, R. (2015). Dynamic alterations to α-actinin accompanying sarcomere disassembly and reassembly during cardiomyocyte mitosis. *PLoS ONE* **10**, e0129176. doi:10.1371/journal.pone.0129176

González-Rosa, J. M., Burns, C. E. and Burns, C. G. (2017). Zebrafish heart regeneration: 15 years of discoveries. *Regeneration* **4**, 105-123. doi:10.1002/reg2.83

Harikumar, A. and Meshorer, E. (2015). Chromatin remodeling and bivalent histone modifications in embryonic stem cells. *EMBO Rep.*. **16**, 1609-1619. doi:10.15252/embr.201541011

Huang, D. W., Sherman, B. T. and Lempicki, R. A. (2009a). Systematic and integrative analysis of large gene lists using DAVID bioinformatics resources. *Nat. Protoc.* **4**, 44-57. doi:10.1038/nprot.2008.211

Huang, D. W., Sherman, B. T. and Lempicki, R. A. (2009b). Bioinformatics enrichment tools: paths toward the comprehensive functional analysis of large gene lists. *Nucleic Acids Res.* **37**, 1-13. doi:10.1093/nar/gkn923

Jopling, C., Sleep, E., Raya, M., Martí, M., Raya, A. and Izpisúa-Belmonte, J. C. (2010). Zebrafish heart regeneration occurs by cardiomyocyte dedifferentiation and proliferation. *Nature* **464**, 606-609. doi:10.1038/nature08899

Kikuchi, K., Holdway, J. E., Werdich, A. A., Anderson, R. M., Fang, Y., Egnaczyk, G. F., Evans, T., MacRae, C. A., Stainier, D. Y. R. and Poss, K. D. (2010). Primary contribution to zebrafish heart regeneration by gata4(+) cardiomyocytes. *Nature* **464**, 601-605. doi:10.1038/nature08804

Kwan, K. M., Fujimoto, E., Grabher, C., Mangum, B. D., Hardy, M. E., Campbell, D. S., Parant, J. M., Yost, H. J., Kanki, J. P. and Chien, C.-B. (2007). The Tol2kit: a multisite gateway-based construction kit for Tol2 transposon transgenesis constructs. *Dev. Dyn.* **236**, 3088-3099. doi:10.1002/dvdy.21343

Laflamme, M. A. and Murry, C. E. (2011). Heart regeneration. *Nature* **473**, 326-335. doi:10.1038/nature10147

Lewis, P. W., Müller, M. M., Koletsky, M. S., Cordero, F., Lin, S., Banaszynski, L. A., Garcia, B. A., Muir, T. W., Becher, O. J. and Allis, C. D. (2013). Inhibition of PRC2 activity by a gain-of-function H3 mutation found in pediatric glioblastoma. *Science* **340**, 857-861. doi:10.1126/science.1232245

Li, H. and Durbin, R. (2009). Fast and accurate short read alignment with Burrows-Wheeler transform. *Bioinformatics* **25**, 1754-1760. doi:10.1093/bioinformatics/btp324

Livak, K. J. and Schmittgen, T. D. (2001). Analysis of relative gene expression data using real-time quantitative PCR and the 2−ΔΔCT method. *Methods* **25**, 402-408. doi:10.1006/meth.2001.1262

Love, M. I., Huber, W. and Anders, S. (2014). Moderated estimation of fold change and dispersion for RNA-seq data with DESeq2. *Genome Biol.*. **15**, 550. doi:10.1186/s13059-014-0550-8

Marro, J., Pfefferli, C., de Preux Charles, A.-S., Bise, T. and Jaźwińska, A. (2016). Collagen XII contributes to epicardial and connective tissues in the zebrafish heart during ontogenesis and regeneration. *PLoS ONE* **11**, e0165497. doi:10.1371/journal.pone.0165497

Natarajan, N., Abbas, Y., Bryant, D. M., González-Rosa, J. M., Sharpe, M., Uygur, A., Cocco-Delgado, L. H., Ho, N. N., Gerard, N. P., Gerard, C. J. et al. (2018). Complement receptor C5aR1 plays an evolutionarily conserved role in successful cardiac regeneration. *Circulation* **137**, 2152-2165. doi:10.1161/CIRCULATIONAHA.117.030801

O'Meara, C. C., Wamstad, J. A., Gladstone, R. A., Fomovsky, G. M., Butty, V. L., Shrikumar, A., Gannon, J. B., Boyer, L. A. and Lee, R. T. (2015). Transcriptional reversion of cardiac myocyte fate during mammalian cardiac regeneration. *Circ. Res.* **116**, 804-815. doi:10.1161/CIRCRESAHA.116.304269

Paige, S. L., Thomas, S., Stoick-Cooper, C. L., Wang, H., Maves, L., Sandstrom, R., Pabon, L., Reinecke, H., Pratt, G., Keller, G. et al. (2012). A temporal chromatin signature in human embryonic stem cells identifies regulators of cardiac development. *Cell* **151**, 221-232. doi:10.1016/j.cell.2012.08.027

Pfefferli, C. and Jaźwińska, A. (2017). The careg element reveals a common regulation of regeneration in the zebrafish myocardium and fin. *Nat. Commun.* **8**, 15151. doi:10.1038/ncomms15151

Porrello, E. R., Mahmoud, A. I., Simpson, E., Hill, J. A., Richardson, J. A., Olson, E. N. and Sadek, H. A. (2011). Transient regenerative potential of the neonatal mouse heart. *Science* **331**, 1078-1080. doi:10.1126/science.1200708

Poss, K. D., Wilson, L. G. and Keating, M. T. (2002). Heart regeneration in zebrafish. *Science* **298**, 2188-2190. doi:10.1126/science.1077857

Quinlan, A. R. and Hall, I. M. (2010). BEDTools: a flexible suite of utilities for comparing genomic features. *Bioinformatics* **26**, 841-842. doi:10.1093/bioinformatics/btq033

Raya, A., Koth, C. M., Büscher, D., Kawakami, Y., Itoh, T., Raya, R. M., Sternik, G., Tsai, H.-J., Rodríguez-Esteban, C. and Izpisúa-Belmonte, J. C. (2003). Activation of Notch signaling pathway precedes heart regeneration in zebrafish. *Proc. Natl. Acad. Sci. USA* **100** Suppl. 1, 11889-11895. doi:10.1073/pnas.1834204100

Sallin, P., de Preux Charles, A.-S., Duruz, V., Pfefferli, C. and Jaźwińska, A. (2015). A dual epimorphic and compensatory mode of heart regeneration in zebrafish. *Dev. Biol.* **399**, 27-40. doi:10.1016/j.ydbio.2014.12.002

Sánchez-Iranzo, H., Galardi-Castilla, M., Sanz-Morejón, A., González-Rosa, J. M., Costa, R., Ernst, A., Sainz de Aja, J., Langa, X. and Mercader, N. (2018). Transient fibrosis resolves via fibroblast inactivation in the regenerating zebrafish heart. *Proc. Natl. Acad. Sci. USA* **115**, 4188-4193. doi:10.1073/pnas.1716713115

Simon, J. A. and Kingston, R. E. (2013). Occupying chromatin: Polycomb mechanisms for getting to genomic targets, stopping transcriptional traffic, and staying put. *Mol. Cell* **49**, 808-824. doi:10.1016/j.molcel.2013.02.013

Vivien, C. J., Hudson, J. E. and Porrello, E. R. (2016). Evolution, comparative biology and ontogeny of vertebrate heart regeneration. *NPJ Regen. Med.* **1**, 16012. doi:10.1038/npjregenmed.2016.12

Venneti, S., Garimella, M. T., Sullivan, L. M., Martinez, D., Huse, J. T., Heguy, A., Santi, M., Thompson, C. B. and Judkins, A. R. (2013). Evaluation of histone 3 lysine 27 trimethylation (H3K27me3) and enhancer of Zest 2 (EZH2) in pediatric glial and glioneuronal tumors shows decreased H3K27me3 in H3F3A K27M mutant glioblastomas. *Brain Pathol.* **23**, 558-564. doi:10.1111/bpa.12042

Wamstad, J. A., Alexander, J. M., Truty, R. M., Shrikumar, A., Li, F., Eilertson, K. E., Ding, H., Wylie, J. N., Pico, A. R., Capra, J. A. et al. (2012). Dynamic and coordinated epigenetic regulation of developmental transitions in the cardiac lineage. *Cell* **151**, 206-220. doi:10.1016/j.cell.2012.07.035

Wang, J., Karra, R., Dickson, A. L. and Poss, K. D. (2013). Fibronectin is deposited by injury-activated epicardial cells and is necessary for zebrafish heart regeneration. *Dev. Biol.* **382**, 427-435. doi:10.1016/j.ydbio.2013.08.012

Wills, A. A., Holdway, J. E., Major, R. J. and Poss, K. D. (2008). Regulated addition of new myocardial and epicardial cells fosters homeostatic cardiac growth and maintenance in adult zebrafish. *Development* **135**, 183-192. doi:10.1242/dev.010363

Zhang, R., Han, P., Yang, H., Ouyang, K., Lee, D., Lin, Y.-F., Ocorr, K., Kang, G., Chen, J., Stainier, D. Y. R. et al. (2013). In vivo cardiac reprogramming contributes to zebrafish heart regeneration. *Nature* **498**, 497-501. doi:10.1038/nature12322

Zhao, L., Borikova, A. L., Ben-Yair, R., Guner-Ataman, B., MacRae, C. A., Lee, R. T., Burns, C. G. and Burns, C. E. (2014). Notch signaling regulates cardiomyocyte proliferation during zebrafish heart regeneration. *Proc. Natl. Acad. Sci. USA* **111**, 1403-1408. doi:10.1073/pnas.1311705111

Zhou, Y., Cashman, T. J., Nevis, K. R., Obregon, P., Carney, S. A., Liu, Y., Gu, A., Mosimann, C., Sondalle, S., Peterson, R. E. et al. (2011). Latent TGF-β binding protein 3 identifies a second heart field in zebrafish. *Nature* **474**, 645-648. doi:10.1038/nature10094

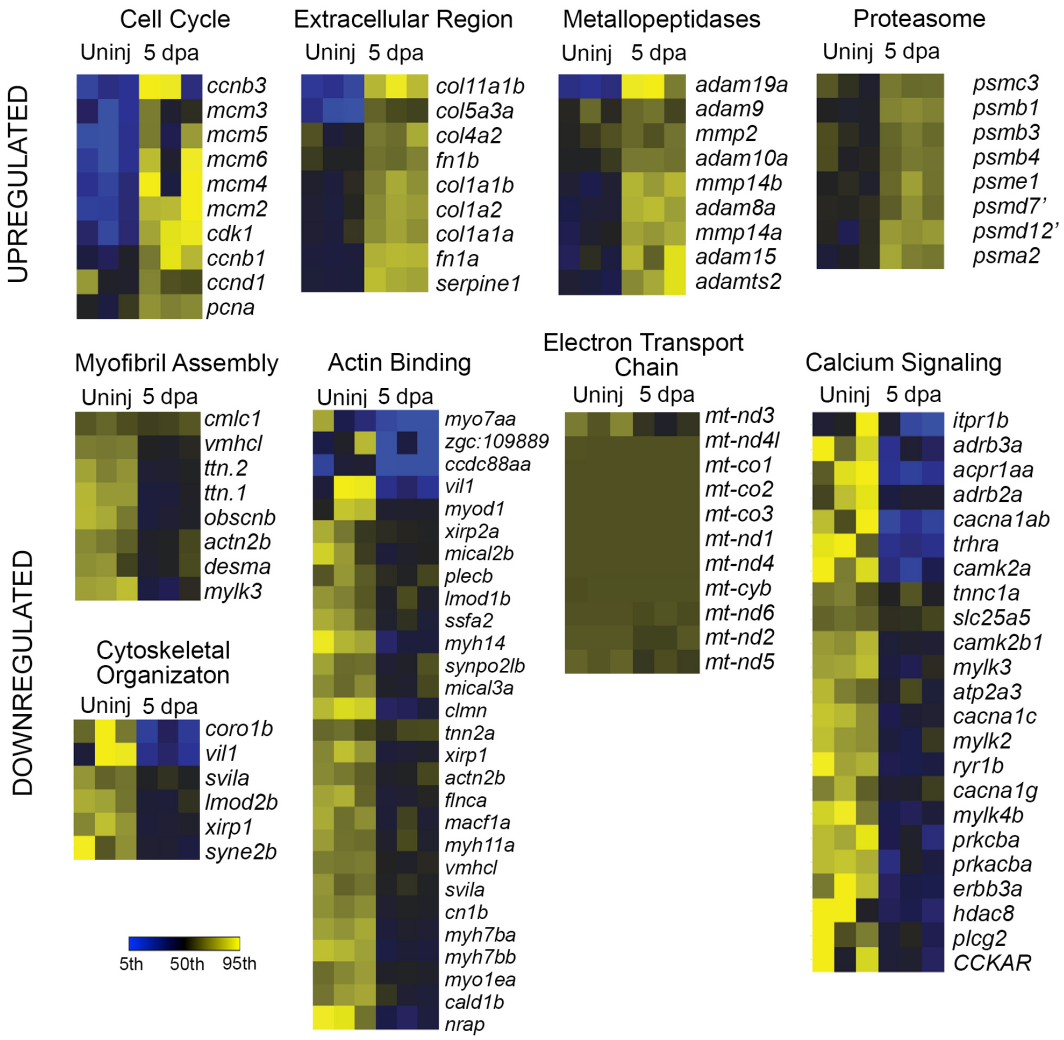

Fig. S1. Gene expression changes accompany cardiomyocyte transitioning from a working to proliferative state following amputation injury to the zebrafish ventricle. (A) Heat maps depicting fold changes for transcripts within specific GO categories showing statistically significant differences between uninjured and 5 dpa GFP+ cardiomyocytes ($p<0.05$). Three biological replicates are shown per cohort. (B) Graphs depicting the lack of fold changes observed for cardiac transcription factor transcripts between uninjured and 5dpa GFP+ cardiomyocytes ($p>0.05$).

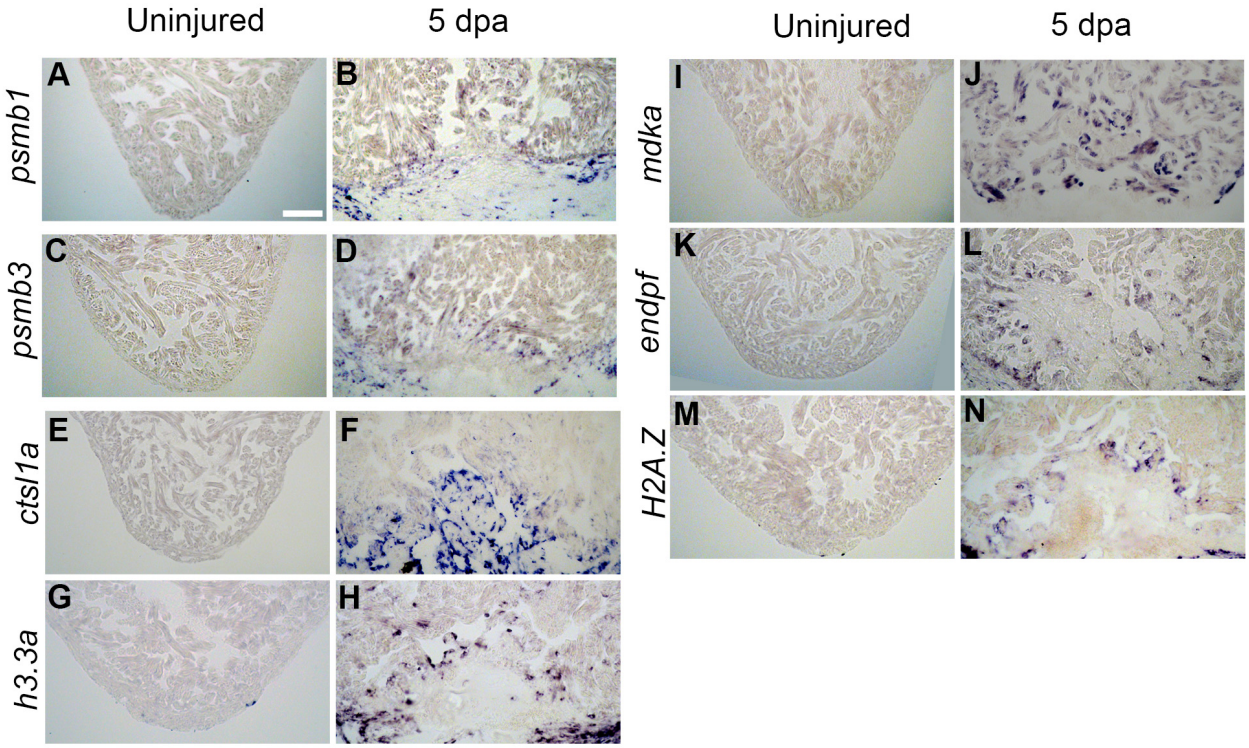

Fig. S2. Spatiotemporal expression of transcripts that change following injury are largely localized to the wound region. (a-n) Representative cardiac sections from uninjured or 5 dpa ventricles processed by in situ hybridization for the indicated transcripts. Injury-dependent upregulation of transcripts can be visualized specifically or non-specifically in wound-edge cardiomyocytes. Scale bar = 80 μm

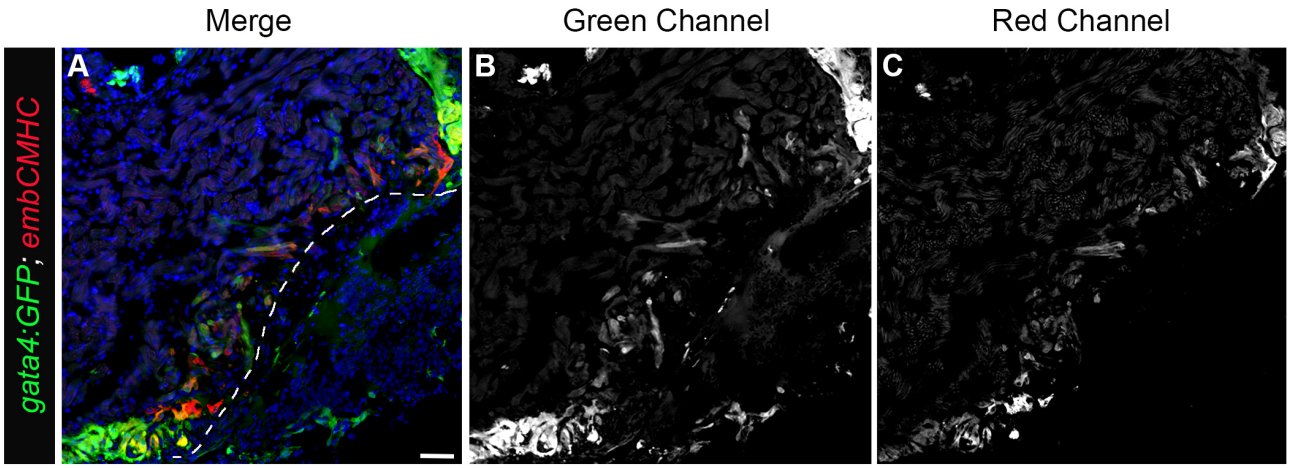

Fig. S3. embCMHC expression overlaps with GFP expression in wound-edge CMs of amputated *gata4:GFP* hearts. (A-C) Representative section of a 5 dpa *gata4:GFP* ventricle co-immunostained for GFP (green) and embCMHC (red) with merged (A) and split channel views (B,C). Dotted line represents the amputation plane. Scale bar = 45 μm

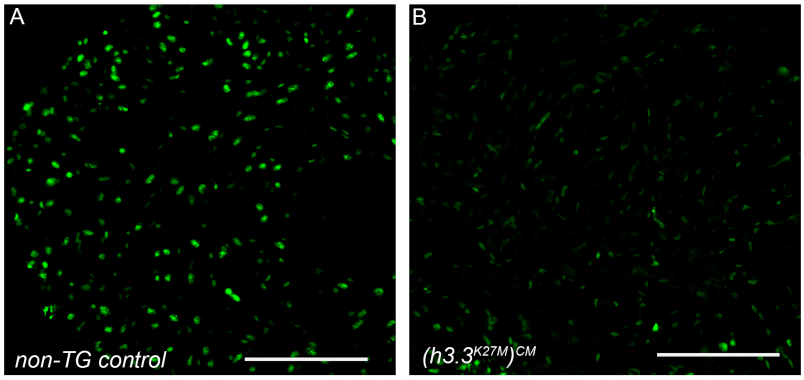

Fig. S4. H3K27me3 levels in heat shocked non-transgenic and *(h3.3^{K27M})^{CM}* hearts. Representative sections of uninjured ventricles following heat-shock treatment and immunostaining for H3K27me3 in non-transgenic and *(h3.3^{K27M})^{CM}* hearts. Scale bar = 100 μm

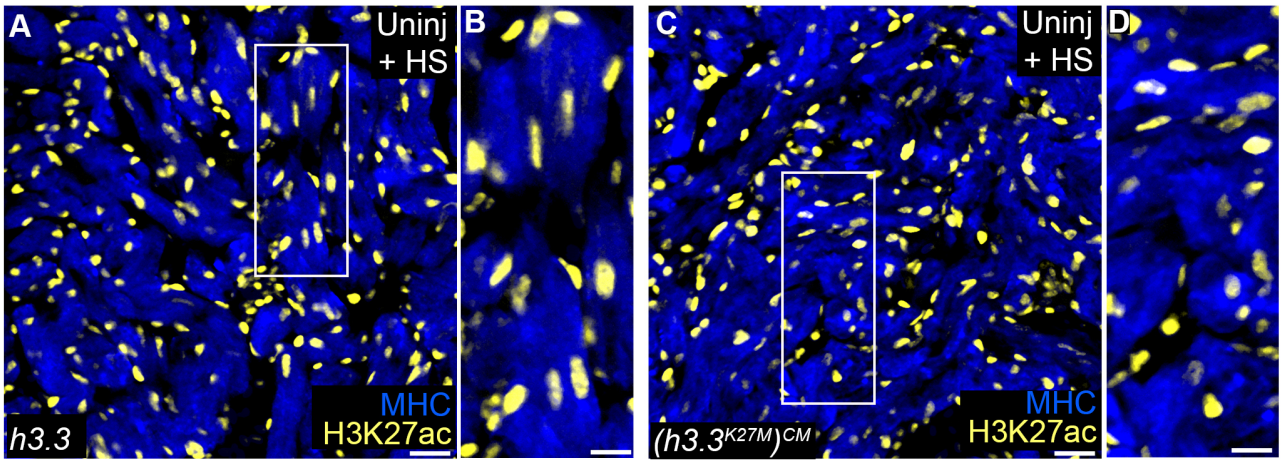

Fig. S5. No change in gross levels of H3K27ac are detected in cardiomyocytes in the presence of *(h3.3^{K27M})^{CM}*. (A-D) Representative sections through an uninjured, heat-shocked control (A,B) or *(hsp70:h3.3^{K27M})^{CM}* (C,D) ventricle stained for H3K27ac (yellow) and myosin heavy chain (blue). Boxed regions in A,C are shown at higher magnification in B,D. Scale bars = 20 μm (A,C); 10 μm (B,D)

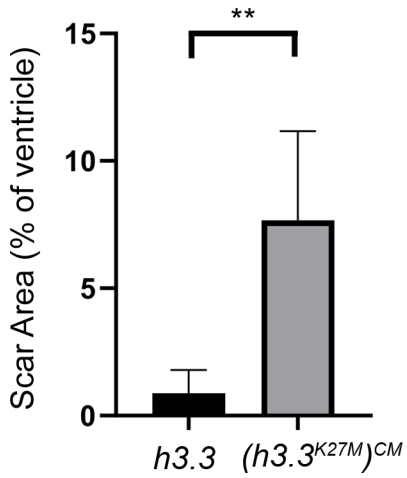

Fig. S6. Quantification of scar size relative to the ventricle. Graph showing the percentages of total ventricular area occupied by scar tissue in 60 days post amputation h3.3 control (n=9) and *(h3.3^{K27M})^{CM}* (n=7) hearts. Scar percentage data were collected for 6-10 sections per heart and averaged to generate each data point. Statistical significance was determined using unpaired two-tailed Student's t-test. **, $p<0.01$.

Table S1. Gene-level expression and differential expression analysis of uninjured and 5 day post-amputation heart samples (corresponds to Fig 1F)

Click here to Download Table S1

Table S2. Gene Ontology analysis of differentially-expressed genes (corresponds to Fig 1G)

Click here to Download Table S2

Table S3. Integrated analysis of epigenetic and transcriptional changes following cardiac injury (corresponds to Fig 1K)

Click here to Download Table S3

Table S4. Gene Ontology analysis of genes displaying epigenetic and transcriptional modulation following cardiac injury (corresponds to Fig 1K)

Click here to Download Table S4

Table S5. Primer sequences

Gene	qPCR primers
ttn.1	AGCTCAAGTTAGTGGTAATCCAGTT; AGAGCGGCAGCAGTAAGAAC
ttn.2	CTGCTGCAAGGTCTTTCTGA; CTGAGAGAATCGCACCTCAA
vmhcl	GATGGAACTGAGGATGCTGAC; TTGACTCTTGGATGGCACAG
flnca	CAATAGACAGCAAAGCCATTGT; GGAGAATAAGCGTCCAGATGA
cmlc1	GCTCTGGGTCACAACCCTAC; GGCAGGAACGTCTCAAAGTC
actb2	GCCTGACGGACAGGTCAT; ACCGCAAGATTCCATACCC
	RNA probe primers
psmb1	ATGATTTCTGCCCAGGCTTAT; CTCCACGTTCTCCATGTTCTT
psmb3	GCGCTTGAAAGAAAGTGTGTAG; GCCTGTGAGATGGTCTCAAATA
h3.3a	ATGGCCCGTACTAAGCAGACCG; TTAAGCCCTCTCTCCTCTGATTCGC
h2afvb	AAGAGAAGCAGCTCATCTGG; CAACAGATTCCTTGCAGCAC
ctsl1a	CACCTACAGACTCGGAATGAAC; CATCAACATCCTCACCCTCAA
mdka	GCCCTCTGAATCTCTCGTTATG; TCCTAACGTCGTGAAGGATTTC
endpf	GGCTGAGGGTTTCCATCTAAG; CGTTGATGTCCTGATCTGATGT
	Cloning primers
h3.3a	ATGGCCCGTACTAAGCAGACCG; TTAAGCCCTCTCTCCTCTGATTCGC
h3.3a (used to generate K27M)	TGAGCGCGCCCTCTACTGGAG; TCCTGGCGGCTTTAGTTGCC